Journal of Nuclear Materials 463 (2015) 818–821

Contents lists available at ScienceDirect

Journal of Nuclear Materials

journal homepage: www.elsevier.com/locate/jnucmat

Analysis of rotating collectors from the private region of JET with carbon wall and metallic ITER-like wall

J. Beal [a,b,c,*], A. Widdowson [a,c], K. Heinola [a,c,d], A. Baron-Wiechec [a,c], K.J. Gibson [a,b], J.P. Coad [a,e], E. Alves [a,f], B. Lipschultz [a,b], A. Kirschner [a,g], G.F. Matthews [a,c], S. Brezinsek [a,g], JET-EFDA Contributors [a,1]

[a] JET-EFDA, Culham Science Centre, Abingdon, OX14 3DB, UK
[b] York Plasma Institute, Department of Physics, University of York, Heslington, York YO10 5DD, UK
[c] Culham Centre for Fusion Energy, Abingdon OX14 3DB, UK
[d] University of Helsinki, PO Box 43, 00014 University of Helsinki, Finland
[e] VTT Technical Research Centre of Finland, PO Box 1000, 02044 VTT Espoo, Finland
[f] Instituto de Plasmas e Fusão Nuclear, Instituto Superior Técnico, Universidade de Lisboa, Avenue Rovisco Pais, 1049-001 Lisboa, Portugal
[g] Forschungszentrum Jülich, Institut für Energie- und Klimaforschung Plasmaphysik, 52425 Jülich, Germany

ARTICLE INFO

Article history:
Available online 5 October 2014

ABSTRACT

Rotating collectors are used in JET to provide time-resolved measurements of erosion and redeposition of vessel materials. The silicon collecting discs rotate behind an aperture, driven by pulsing of the toroidal magnetic field, with the deposits analysed ex-situ by nuclear reaction analysis. The angular dependence of deposition is mapped to discharge number using the B-field history, allowing the influence of different plasma configurations and parameters to be investigated. A simple geometrical model using sputtering and reflection from the strike point has qualitatively reproduced the deposition found on collectors located under the central divertor tile and facing towards the inner strike point. The beryllium deposition on the ITER-like wall (ILW) collector showed an order of magnitude reduction in deposition compared to carbon deposition on the JET-C collector. This decreased deposition is attributed to low long range divertor transport due to reduced chemical sputtering/erosion and codeposition of beryllium relative to carbon.

1. Introduction

Erosion, deposition and material migration are of critical importance both for the lifetime of tokamak first wall components and for their impact on plasma behaviour. The nature and degree of physical, chemical and thermal plasma–material interactions are strongly dependent on the material composition of the plasma-facing surfaces. In 2010, the carbon wall of JET-C was replaced with a beryllium main chamber and tungsten divertor. This ITER-like wall (ILW) [1] has provided the first complete test of the plasma-facing material combination proposed for ITER. The exchange caused an almost complete replacement of carbon in the plasma by beryllium [2]. Thus, we assume here only carbon impurities in the carbon case and beryllium impurities in the ILW case.

Since detailed material analysis of plasma-facing components is generally only practical ex-situ, data on the evolution of surfaces typically has the time resolution of a 1–2 year operating campaign. By varying the surface exposed to the plasma, rotating collectors offer an improved time resolution and thereby enable an investigation of the effects of changing plasma conditions. This contribution focuses on deposition measurements from rotating collectors located in the private-flux region of the JET divertor during 2005–12, and analyses them in terms of plasma conditions and first wall composition.

2. Experimental

Since a detailed explanation of rotating collectors is offered in [3], only a brief description is provided here. Each collector comprises a silicon disc that acts as a substrate for deposition, incrementally rotated via a geared drive by the pulsing of the toroidal magnetic field. A slit in the collector housing exposes a 2 mm toroidal strip on the circumference of the disc at any given time. This corresponds to ~55 times the circumferential distance rotated each JET discharge, resulting in a moving sum of deposition on the disc. The angular deposits are mapped to discharge number, neglecting those discharges with insufficient magnetic field to drive rotation.

* Corresponding author at: Culham Science Centre, Abingdon OX14 3DB, UK.
E-mail address: James.Beal@ccfe.ac.uk (J. Beal).
[1] See the appendix of F. Romanelli et al., Proc. 24th IAEA Fusion Energy Conference 2012, San Diego, US.

http://dx.doi.org/10.1016/j.jnucmat.2014.09.069
0022-3115/

Between campaigns, the collectors are retrieved and analysed ex-situ by nuclear reaction analysis (NRA). An incident beam of 2.3–2.5 MeV ^{3}He ions allows the simultaneous quantification of carbon, beryllium and deuterium on the collectors via the ^{12}C(^{3}He, p)^{14}N, ^{9}Be(^{3}He, p)^{11}B and ^{2}H(^{3}He, p)^{4}He reactions. Fig. 1 depicts the geometry of the rotating collector considered here. Thermocouples in this region under the central divertor tile indicate local temperatures of ~80–150 °C. The recessed position and view of the inner divertor give a deposition-dominated location, suited to investigation of transport to remote areas and strike point locations.

3. Modelling

Erosion, deposition and material migration in JET have previously been studied using models such as the 3-D Monte Carlo code ERO [4], which provides a detailed treatment of plasma–surface interaction and transport processes. The approach here differs in its increased emphasis on long term changes in erosion/deposition and increased use of experimental data. Since the whole collector lifetime of thousands of pulses is modelled, transport is necessarily simplified using line of sight assumptions. Sputter cones of eroded material are generated at the strike point, with the deposition on the collector calculated geometrically and a 55 discharge moving sum applied. While it is hoped that the model achieves tolerable quantitative agreement with experimental depositions, the primary interest is the evolution of the deposition profile as a function of the varying plasma conditions during campaigns. This focus on the changes in deposition and the assumptions made mean that the magnitude of the deposition profile requires scaling by a (constant, <1) attenuation factor. This describes the ratio of the material that deposits on the collector surface to that which leaves the tile surface travelling towards the collector aperture. The approach used is to find the factor that best fits to the experimental deposition, followed by an examination of the reasonableness and implications of such a value.

For the JET-C case, carbon may be eroded from the main chamber and transported to the divertor, forming hydrocarbon layers that are re-eroded by incident deuterium and re-deposited in remote areas [5]. Similarly, in the ILW case, beryllium may be eroded from the main chamber and deposit/re-erode in the divertor. The re-erosion from the inner strike point is modelled, with its location determined through use of EFIT equilibrium reconstruction [6] and local Langmuir probe flux profiles. The physical and chemical carbon erosion yields are calculated every ~30 ms EFIT time point using the Roth–Garcia-Rosales formulae, which provide analytical yield equations using fits to experimental and modelling results [7]. These formulae include a treatment of the erosion of weakly bound surface hydrocarbons. The erosion of beryllium is predominantly physical [8], with the physical sputtering yield calculated using the formulae proposed by Eckstein and Preuss [9], which accurately describe the yield at low incident energies close to the threshold.

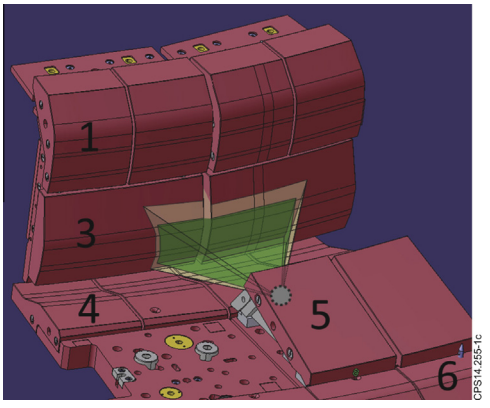

Fig. 1. The MkII-HD (carbon) inner divertor, with tile numbers labelled. The rotating collector is located under central tile 5 and views tile 3. The projections depict the tile locations that have full and partial views of the collector.

In the ILW case, 80% efficient reflection of beryllium from the tungsten divertor is also included [10], assuming an incident flux containing a 0.2% beryllium impurity [2]. The sputtering and reflection contributions to deposition on the collector are not entirely mutually compatible. A tile completely covered with beryllium will maximize the sputtering contribution, but beryllium–beryllium reflection is low. Conversely, low coverage will maximise reflection from the tungsten, but there will be little deposited beryllium available to be sputtered. As such, the mean of the deposition due to the two processes is taken, reflecting the fact that on average they contribute similar magnitudes to the modelled deposition, but cannot be simultaneously maximised.

The calculated yields are functions of the incident energy, ion flux and target temperature. The angle of incidence was assumed to be 60° based on modelled ion trajectories [11], increasing the yield since more energy is deposited in the near-surface region. The incident energy E_i was 50 eV, based on an assumption of $T_e = 10$ eV, $T_i = T_e$ and $E_{in} = 3ZT_e + 2T_i$, with electron temperature T_e, ion temperature T_i and atomic number Z. Tile surface temperatures were estimated using a linear, temporal fit of thermocouple measurements to selected IR thermography data, typically giving temperatures ~450–700 K. Ion fluxes from local Langmuir probes were used as inputs to the yield calculations, and were multiplied by the resulting yields to give the sputtering source. Since for most ILW conditions physical sputtering is expected to be dominant, the constant ion energy assumption is more vulnerable to deviations causing variations in yields. While there are changes in this and in the impurity content for individual discharges, the smoothing resulting from the finite collector slit width makes the constant assumptions reasonable approximations.

At each time point, cosine cones of sputtered/reflected particles are generated from the target, with the peak shifted 30° poloidally below the tile surface normal to preserve some of the directionality of the incident ions. The upper and lower line of sight acceptance angles to the collector are calculated for each strike point, with deposition calculated by integrating the cones between these bounds. Strike points with no line of sight to the collector (e.g. those on tile 4) are neglected, save for the application of a small background re-erosion from the collector surface. Quartz Micro Balance (QMB) measurements have shown that moving the strike point from tile 3 to 4 changes this from a deposition-dominated to an erosion-dominated region [12].

4. Results

The results from the 2005–07 rotating collector have previously been published in [3]. This data is plotted in Fig. 2 with the results of the geometric model, showing considerable qualitative agreement. The modelled results have been scaled by an attenuation factor of 0.12, describing the efficiency of transport of sputtered particles. The model's over-estimate of deposition after discharge 66,000 suggests a physical reduction in this parameter later in the campaign. For the 2007–09 period, configurations generally varied over shorter periods than the 55 discharge (~2 days) resolution, but broad features of the deposition and dependence on plasma configurations are identifiable. Table 1 shows that though the deposition per pulse was reduced by a factor of ~2, much of this was due to decreased line of sight time to the collector (Fig. 3). The increased strike point time on tile 4 for 2007–09 implies that the remaining difference may be due to increased re-erosion from the collector surface [12].

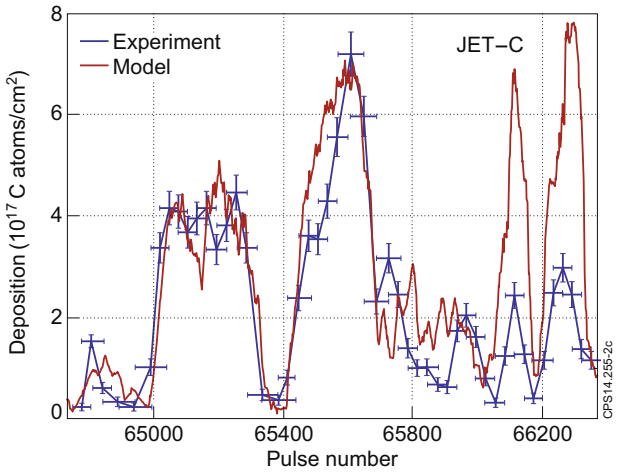

Fig. 2. Carbon deposition on the rotating collector for the 2005–07 carbon campaign found by NRA (blue), and model scaled by 0.12 attenuation factor (red). The NRA measurement process is Poissonian, giving $n^{-1/2}$ errors on the deposition. The pulse number error bars show the bounds of the moving sum of deposition imposed by the finite slit width.

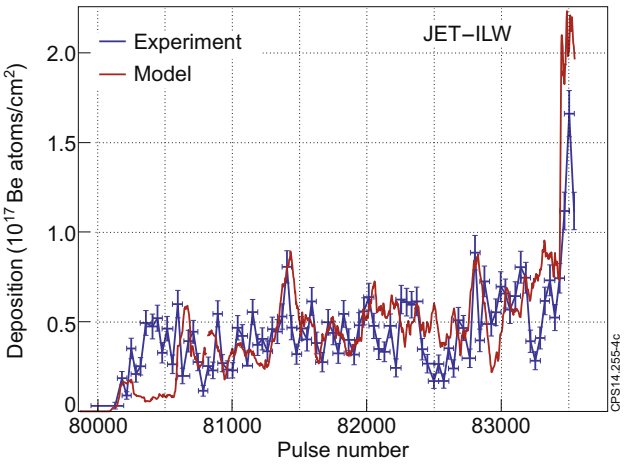

Fig. 4. Beryllium deposition on the collector for 2010–12 ILW operation found by NRA (blue), and model scaled by 0.64 attenuation factor (red). The larger final horizontal error bar indicates that the collector ended its rotation before the end of the campaign, resulting in high aggregate deposition. The modelled deposition for the remaining pulses has been allocated to this stopping point accordingly.

Table 1
Average deposition on collectors per pulse and per second of time the strike point had a line of sight (LOS) to the collector. The last column shows the equivalent beryllium deposition rates after normalising to the solid angle Ω subtended by the carbon collectors.

Campaign	05–07	07–09	10–12	10–12 (Ω)
Impurity	C	C	Be	Be
Deposition/pulse 10^{15} at/cm^2	6.89	3.18	0.79	0.44
Deposition/LOS time 10^{15} at/cm^2/s	0.82	0.63	0.09	0.05

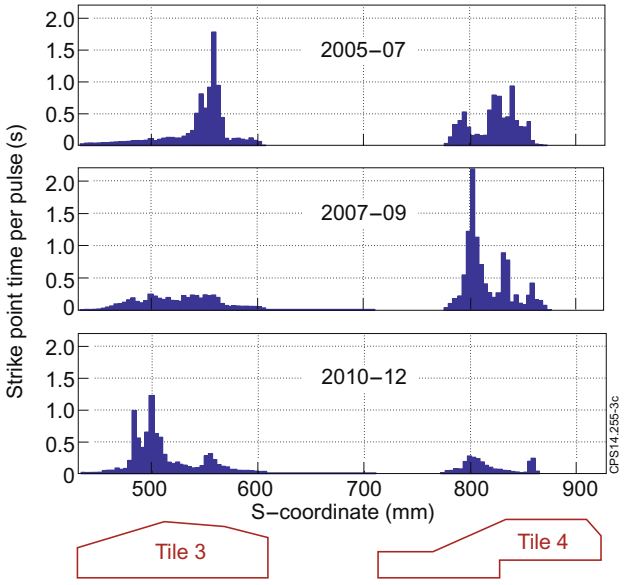

Fig. 3. Campaign-averaged inner strike point distributions. The S-coordinate system follows the divertor surface poloidally. For 2010–12 operation there were also a significant number of strike points on tile 1, part of which has an acute line of sight to the collector for the ILW geometry.

The measured and modelled (with attenuation factor 0.64) beryllium deposition on the 2010–12 ILW collector is shown in Fig. 4. There is reasonable qualitative agreement, though the relative lack of distinctive features makes comparison harder. The profile is more constant than for the carbon case, though there is some variation mostly due to changes in ion fluxes and strike points. Table 1 shows that the ILW deposition rate as a function of line of sight time was reduced by a factor of 7–9 relative to JET-C, and by 13–17 when normalised to the larger solid angle subtended by the JET-C collector.

5. Discussion

5.1. Carbon

The agreement between the modelled and experimental results supports previous work showing that line of sight divertor transport from the strike point to remote regions is the dominant process [13]. The large mean free paths of the sputtered neutrals in the private-flux region imply that most losses of sputtered particles are likely due to ionization and redeposition near their point of origin, before crossing the separatrix. If the attenuation factor of 0.12 is solely due to this local redeposition, the redeposition rate of 0.88 is comparable to rates found from ERO modelling [14].

After discharge 66,000 there are still strong time variations in collector deposition, but the magnitude is lower than that found by the model with its fixed attenuation factor (though the right time dependence is preserved). After this point, there were a greater fraction of high power/ELMy discharges, leading to higher divertor radiated powers and suggesting a higher heat flux to and surface temperature of the collector. This may cause a reduction in the deposition efficiency and change the structure of the deposited layers. Increased surface temperature has been found to decrease deposition on QMBs [3] (though the collector is less thermally isolated, suggesting a smaller temperature rise). ELMs may also drive the formation of particle clusters, which could dominate the material migration during ELMs due to their longer mean free paths and change the deposition characteristics [16]. An examination of the ion flux and D-alpha signals in the inner divertor indicates increased detachment in the inner divertor later in the campaign. Though the reduced ion flux during detachment is accounted for in the model through use of Langmuir probe data, detachment may also reduce the physical and chemical sputtering yields [16]. Finally, higher power discharges may cause enhanced re-erosion from the collector surface, reducing the net deposition.

5.2. ILW

The reduction in the beryllium deposition rate on the ILW collector by a factor of 13–17, relative to carbon deposition on the JET-C collectors, is consistent with an observed order of magnitude reduction in both overall ILW divertor deposition [17] and integral deposition on QMBs similarly located under tile 5 [18]. This reduced deposition demonstrates the low long range migration of beryllium in the ILW divertor due to negligible chemical erosion and decreased chemical sputtering and codeposition of beryllium relative to carbon [8]. The attenuation factor of 0.64 implies a redeposition fraction of 0.36, which is comparable to rates found using ERO [10].

For ILW operation, the deuterium ions generally have insufficient energy to sputter the tungsten tiles, with most of the erosion occurring due to ELMs or sputtering by incident beryllium [19]. Because of this, the tungsten deposition on the collector was approximately two orders of magnitude below that of beryllium, with low deposition levels of $\sim 8 \times 10^{12}$ W atoms/cm^2/pulse identified using Rutherford Backscattering Spectrometry (RBS). Though there were deposits of $\sim 8 \times 10^{13}$ C atoms/cm^2/pulse of carbon measured on the ILW collector, these did not correlate with deuterium deposition, suggesting that codeposition of carbon with deuterium is not dominant in this location of the JET-ILW. This contrasts with the JET-C case, where the D/C ratio stayed close to 1. For the ILW collector, the D/Be ratio generally decreased during the campaign from ~1 to ~0.25. This is attributed to higher power discharges causing increased collector surface temperatures via increased heat fluxes to the collector and thermal conduction through tile 5. Empirical scaling equations for deuterium retention in beryllium deposits [20] indicate that this decrease is compatible with a moderate temperature increase of ~100 K.

The prevalence of configurations with strike points on tile 3 (Fig. 3) contributed to less temporal variation of deposition on the ILW collector. Although post-mortem analysis indicates permanent deposits on tile 3 are low to zero [17], the beryllium coverage may be expected to vary dynamically during the campaign, causing sputtering and reflection to contribute varying proportions to the deposition. However, both mechanisms depend on geometrical line of sight transport from the strike point. In addition, the opposite dependences of sputtering and reflection on coverage and (1 – coverage) respectively suggests that they are mutually limiting. This is expected to partially neutralise the dependence of deposition on coverage, making it hard to extricate the two mechanisms. However, beryllium deposits have been shown to accumulate on divertor tiles during the ~30 limiter discharges at the start of the ILW campaign, before divertor discharges began [21]. It is noted that the deposition found on the collector experimentally exceeds that expected from the model for the first ~400 (divertor) discharges. This relatively large deposition suggests a strong sputtering contribution from tile 3, which dominates during this period due to the initial conditions of high beryllium coverage.

6. Conclusions

The time-resolved deposition on rotating collectors in a remote location with a line of sight to the JET inner divertor has been investigated for carbon and ILW operation. A simple geometrical model using experimental data has been shown to qualitatively reproduce the deposition on the collectors. The deposition is dependent on variations in strike point locations and other operating conditions. The deposition rate on the ILW collector is reduced by a factor of 13–17 relative to carbon operation. This decreased deposition in remote locations is indicative of the low long range divertor transport found with an all metal wall due to reduced chemical sputtering/erosion and codeposition. Future work will develop the modelling and understanding of deposition in this and other vessel locations, highlighting the consequences of the change from JET-C to JET-ILW.

Acknowledgements

This work was supported by EURATOM and carried out within the framework of the European Fusion Development Agreement. The views and opinions expressed herein do not necessarily reflect those of the European Commission.

References

[1] G.F. Matthews et al., Phys. Scr. T145 (2011) 014001.
[2] S. Brezinsek et al., J. Nucl. Mater. 438 (2013) S303–S308.
[3] J.P. Coad et al., Phys. Scr. T138 (2009) 014023.
[4] A. Kirschner et al., Nucl. Fusion 40 (2000) 989.
[5] M. Mayer et al., Phys. Scr. T111 (2004) 55.
[6] L.L. Lao et al., Nucl. Fusion 30 (1990) 1035.
[7] J. Roth, C. Garcia-Rosales, Nucl. Fusion 36 (1996) 1647.
[8] S. Brezinsek, These Proceedings.
[9] W. Eckstein, R. Preuss, J. Nucl. Mater. 320 (2003) 209.
[10] A. Kirschner et al., These Proceedings.
[11] K. Schmid et al., Nucl. Fusion 50 (2010) 105004.
[12] H.G. Esser et al., J. Nucl. Mater. 390–391 (2009) 148.
[13] J.P. Coad et al., Phys. Scr. 1999 (1999) 7.
[14] A. Kirschner et al., J. Nucl. Mater. 337–339 (2005) 17.
[15] A. Kreter et al., Phys. Rev. Lett. 102 (2009) 045007.
[16] S. Brezinsek et al., J. Nucl. Mater. 390–391 (2009) 267.
[17] A. Widdowson et al., Phys. Scr. T159 (2014) 014010.
[18] H.G. Esser et al., These Proceedings.
[19] G. van Rooij et al., in: Proc. 24th IAEA Fusion Energy Conf. (FEC2012), San Diego, CA, 2012.
[20] G. de Temmerman et al., Nucl. Fusion 49 (2009) 042002.
[21] K. Krieger et al., J. Nucl. Mater. 438 (2013) S262.